CrystEngComm

Accepted Manuscript

ROYAL SOCIETY OF CHEMISTRY

www.rsc.org/crystengcomm

Journal Name

ARTICLE

In situ X-ray Diffraction Study on the Formation of α-Sn in Nanocrystalline Sn-based Electrodes for Lithium-Ion Batteries

Received 00th January 20xx,
Accepted 00th January 20xx

DOI: 10.1039/x0xx00000x

www.rsc.org/

Nikolas Oehl[a], Guido Schmuelling[b], Martin Knipper[a], Richard Kloepsch[b], Tobias Placke[b], Joanna Kolny-Olesiak[a], Thorsten Plaggenborg[a], Martin Winter[b] and Juergen Parisi[a]

In situ X-ray diffraction (XRD) was performed to study the formation of the α-Sn structure in nanocrystalline Sn-based electrodes during electrochemical lithium insertion and extraction at room temperature. Therefore, pure ß-Sn nanoparticles were synthesised and further processed to electrodes. The lithiation and de-lithiation process of the ß-Sn nanoparticles follows the formation of discrete lithium-tin phases which perfectly fits the voltage plateaus in the charge/discharge diagram. However, unlike bulk electrodes, where no α-Sn is formed, we observed the formation of the semiconducting α-modification at 870 mV *vs.* Li within the first de-lithiation process. This observtion explains earlier reports of an increasing internal resistance of such an electrode. Additionally, our study supports earlier suggestions that predominantly small tin crystallites are transformed from the ß-Sn into the α-Sn phase, while larger crystallites retain their metallic ß-Sn structure.

Introduction

In order to increase the specific energy (Wh kg^{-1}) and energy density (Wh L^{-1}) of lithium-ion batteries, there is a need for high-capacity anode materials to replace graphitic carbons as state-of-the-art negative electrode material. Apart from silicon[1], tin is a promising anode material due to its high gravimetric (959 mAh g^{-1}) and volumetric (2000 mAh cm^{-3}) capacity.[2] Tin nanoparticles can be transformed from the metallic ß-Sn into the semiconducting α-Sn structure at room temperature when cycled in a lithium-ion battery.[3–7] Kim *et al.*[3] reported the existence of cubic Sn (α-Sn) in small (3 – 8 nm) nanoparticles after 30 cycles in a lithium-ion cell. Furthermore, Xu *et al.*[4] investigated the mechanical damage of 10 nm sized Sn nanocrystals during electrochemical reactions with lithium with *ex situ* high resolution transmission electron microscopy (HR-TEM). Their findings show that the Sn nanocrystals were transformed from the tetragonal ß-Sn phase to the cubic α-Sn after lithium insertion and extraction. The authors concluded that the stability of the polymorphs α-/ ß-Sn could be affected by the size of the crystallites. Such size-dependent phase transformations are well-documented in literature, especially for oxides like TiO_2 or Al_2O_3.[8,9] Im *et al.*[5] studied the phase evolution of Sn nanocrystals (7 nm) embedded in a carbon matrix during long-term cycling. They pointed out that the α-/ß-Sn ratio increases with respect to the cycle number. Finally, Oehl *et al.*[7] investigated at which crystallite size the Sn nanoparticles are transformed from the ß- to the α-structure. The critical size was determined to be 17(4) nm for ß-Sn nanocrystals at room temperature. However, these investigations did not address the question, when this transformation occurs. Furthermore, these work did not deal with the lithiation of the α-Sn phase.

In situ X-ray diffraction (XRD) measurements by Rhodes *et al.*[10] on bulk Sn electrodes showed, that the lithiation and de-lithiation process follows discrete lithium-tin phases. The presence of four phases including ß-Sn, Li_2Sn_5, ß-LiSn and $Li_{22}Sn_5$ were identified, which were formed during lithiation and de-lithiation, and could be correlated to the voltage plateaus in the charge/discharge profile. In their work, no α-Sn phase formation was observed.

In this study, we investigate the first cycle lithiation and de-lithiation process of Sn/SnO_x core/shell nanoparticles with an *in situ* XRD technique in order to get an insight into the mechanism of the α-Sn formation. The *in situ* XRD measurements show that the lithiation/de-lithiation process follows similar lithium-tin phases as in Sn bulk electrodes. However, in contrast to the bulk material, the α-Sn phase is formed at the end of the first de-lithiation process at 870 mV vs. Li. Furthermore, the measurements show, that the α-Sn phase gets lithiated contemporaneous with the ß-Sn phase, forming the same Li-Sn phases.

[a] *University of Oldenburg, Energy and Semiconductor Research Laboratory, Institute of Physics, Carl-von-Ossietzky-Str. 9-11, 26129 Oldenburg, Germany*
[b] *University of Muenster, MEET Battery Research Center, Institute of Physical Chemistry, Corrensstr. 46, 48149 Muenster, Germany*

† Electronic Supplementary Information (ESI) available: [cif data of nanoparticle ß-Sn and a-Sn crystal structure]. See DOI: 10.1039/x0xx00000x

Experimental methods

Sn nanoparticles with a volume weighted mean diameter of 24 nm ($D_{4,3}$ = 24 nm) were synthesized following a method reported in one of our previous studies.[11] Briefly, 10 g polyvinylpyrrolidone (PVP, M.W. 40 000 g/mol, Alfa Aesar) and 3.5 g $SnCl_2$ (99%, Sigma-Aldrich) were dissolved at room temperature in 900 mL tetraethylene glycol (TEG, 99% Alfa Aesar). The stirred solution was heated up to 120 °C using Schlenk technique under Argon atmosphere. A freshly prepared solution of 9 g sodium borohydride (NaBH4, 99%, Acros) in 100 mL TEG was added dropwise to the stirred $SnCl_2$ solution. The nanoparticle solution was cooled down to room temperature and diluted with acetone in order to isolate the prepared nanoparticles. The nanoparticles were dispersed and stored in ethanol.

XRD investigations were performed using a Bruker D8 Advance X-ray diffractometer (Bruker AXS GmbH) equipped with a copper target X-ray tube (λ= 1.54 Å). *In situ* XRD analysis of the Sn active material upon galvanostatic cycling was carried out using a self-designed *in situ* cell, which has been described previously.[12] The electrode paste consisting of 80 wt.% Sn nano-particles, 12 wt.% conductive carbon agent Super C65 (Imerys) and 8 wt.% sodium carboxymethylcellulose (Na-CMC) as binder (Walocel CRT 2000 PPA 12, Dow Wolff Cellulosics) was applied onto a beryllium (Be) window serving as both the current collector and X-ray transparent window. Metallic lithium foil (Rockwood Lithium) served as counter electrode, Whatman glass fiber (grade GF/D) as separator and 1 M $LiPF_6$ in EC/DEC 3:7 (by weight) with 2 wt.% VC (UBE) as electrolyte. After resting, the cell was galvanostatically cycled at a current rate of C/15 (based on the tin active weight m = 6.52 mg, theoretical specific capacity = 950 mAh g^{-1}) between 0.025 V and 1.5 V with a constant voltage step at the lower cut-off voltage (I ≤ C/20). Simultaneously, XRD measurements were performed in an angular range of 21-81° 2θ with a step size of 0.015 degrees and a step time of 0.7 s, resulting in 50 minutes per XRD scan at an accelerating voltage of 40 kV and a current of 40 mA. The Rietveld refinement of the diffraction pattern was applied with the Maud software 2.4.9 in the angular range of 21-47° 2θ. The crystal structure parameters for the ß-Sn (03-065-7657) and the α-Sn (01-087-0794) phase were taken from the ICDD database. A polynomial of the fourth degree was used to refine the background; incident intensity factor, lattice constants and crystallite size and strain were refined in a second and a third step.

Results and Discussion

TEM and XRD measurements reveal that the as prepared Sn nanoparticles are spherical (see Figure 1a) and consist of crystalline ß-Sn core and a small amorphous SnO_x shell (see Figure 1b). The nanoparticles show a broad size-distribution from 5 nm to 40 nm (see Figure 1a). This size-distribution is well suited to study the lithiation of ß-Sn as well as the lithiation of the α-Sn phase which is formed already in the first cycle.

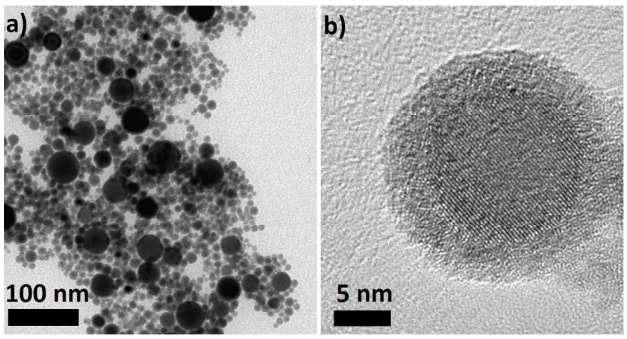

Figure 1: HR-TEM image of the prepared Sn/SnO_x core/shell nanoparticles.

The size-distribution was determined from TEM measurements and reveals a mean diameter of 9.8 nm and a volume-weighted mean diameter of 24 nm. The volume-weighted mean diameter was calculated according to equation 1:

$$D_V = \sum \frac{d^4}{d^3} \quad (1)$$

This size is large enough to get strong reflections for the *in situ* X-ray diffraction measurements and it is small enough to observe the desired ß/α-phase transformation.

A Rietveld refinement with the Maud software version 2.3.3 was applied in order to analyse the diffraction pattern of the as prepared nanoparticles. The crystal structure of Sn and SnO was considered to calculate the diffraction pattern. Figure 2 shows the result of the refinement.

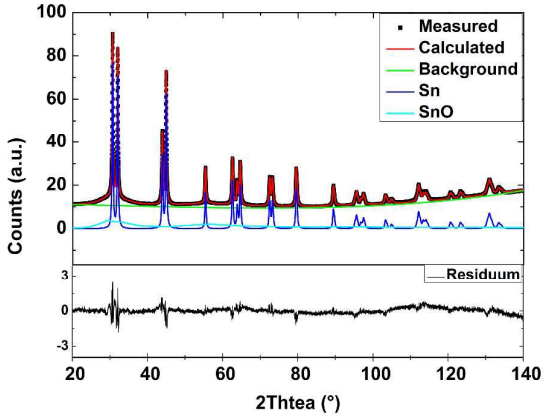

Figure 2: XRD measurement of the prepared Sn/SnO_x nanoparticles and the result of the Rietveld refinement. The weighted R factor is 2.1 %.

All strong reflections in this pattern could be assigned to the ß-Sn phase. A broad peak between 30° and 35° 2Theta can be explained with the SnO_x phase. This strong broadening results from the small crystalline domains of that phase. Therefore we conclude that the nanoparticles consists of a crystalline ß-Sn core and a SnO_x shell with only very small crystalline domains. This conclusion is supported by HR-TEM measurements (Figure 1b) which show a highly crystalline core and an amorphous shell. The results from the refinement of the diffraction pattern of the as prepared nanoparticles are in good agreement with the TEM

Table 1: Summarized structural data from the Rietveld refinement in Figure 5.

	ß-Sn			α-Sn		$w_\alpha/w_ß$ [a]	R_{wp} (%) [b]
	a (Å)	c (Å)	L (nm) [c]	a (Å)	L (nm)		
as prepared	5.8388(1)	3.186(1)	24.6(9)	-	-	-	3.5
after 1st cycle [d]	5.8393(1)	3.188(1)	26(2)	6.467(1)	7.1(4)	0.23	3.4

[a] $w_\alpha/w_ß$ denotes to the weight ratio of α-phase/ß-phase

[b] R_{wp} denotes to the weighted R-factor

[c] L denotes to the crystallite size

[d] in the de-lithiated state

measurements. Figure 3 shows the volume-weighted size-distribution of the as prepared Sn nanoparticles. According to a critical size of 17(4) nm, 33(7) wt.% of the particles should be transformed into the α-modification after electrochemical

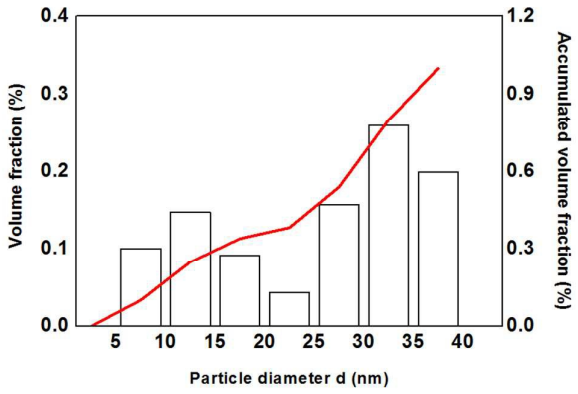

Figure 3: Volume weighted size histogram of the prepared tin nanoparticles determined from TEM measurements.

lithium insertion and extraction. The X-ray diffraction patterns of the *in situ* XRD measurement and the corresponding voltage profile of the first charge/discharge cycle are displayed in Figure 4. The results show that the lithiation process follows the formation of discrete lithium-tin phases, which perfectly correlate with the voltage plateaus from the charge/discharge profile. The lithiation process follows the same lithium-tin phases which are formed in bulk Sn-based electrodes, *i.e.* Li_2Sn_5, LiSn and $Li_{22}Sn_5$.[10] At the beginning, the assembled *in situ* cell has an initial open circuit voltage of 2.78 V and the diffraction pattern only shows the reflections of ß-Sn (Fig. 4a) and the (100) reflection originating from the Be-window at 46.1° 2θ. The transformation of the SnO_x shell into the Li_2O phase is not observed in the X-ray diffraction measurements, because of the small crystalline domain of the shell and the small scattering cross-section between X-rays and light elements. Nevertheless, a small voltage plateau at 0.9 V indicates such a transformation. When the cell voltage reaches the first plateau at 0.56 V, the reflections from the ß-Sn phase vanish and a crystalline Li_2Sn_5 (Fig. 4b) phase is formed. Shortly after the voltage falls below 0.42 V the reflections from Li_2Sn_5 disappear and signals of the LiSn (Fig. 4c) phase appear. Once the voltage decreases below 0.31 V, the characteristic reflections[13,14] (a broad reflection at 22° and a sharp one at 38°) of the highest lithiated phase $Li_{22}Sn_5$ (Fig. 4d) occur. In some literature reports, $Li_{17}Sn_4$ was identified as the highest

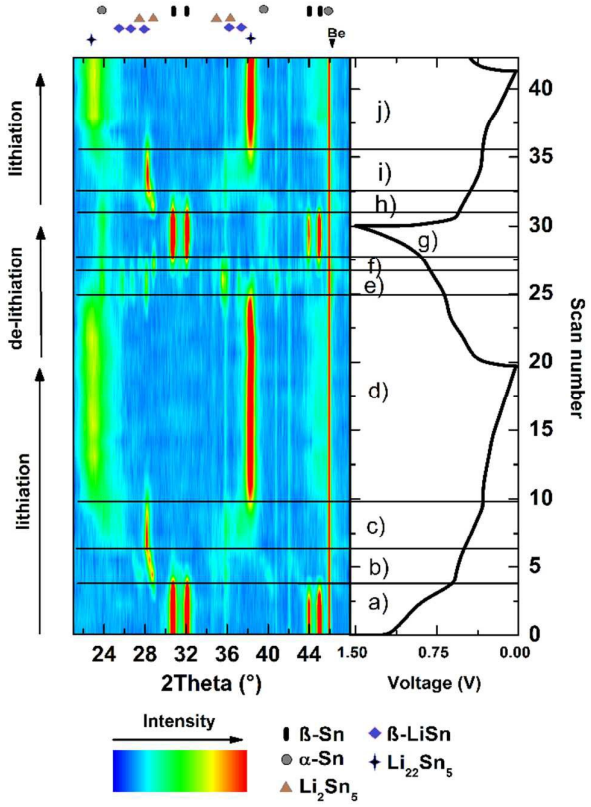

Figure 4: Isoplot of the *in situ* XRD measurement taken during the first charge/discharge cycle of the Sn nanoparticle-based electrode. Characteristic reflections of the relevant phases are marked. The voltage profile is plotted to the right and black lines were drawn to denote a phase transformation.

lithiated phase.[15] Nevertheless, the $Li_{17}Sn_4$ crystal structure does not fit to the XRD pattern from the highest electrochemically lithiated Sn phase in our experiment.

During de-lithiation (Fig. 4d-g), the same lithium-tin phases appear and vanish in reverse order and with more overlap between diffraction peaks representing the various phases. However, an uprising phase can still be correlated to a new plateau in the voltage profile.When the voltage exceeds 0.87 V, the reflections from ß-Sn return, and additionally, reflections of α-Sn (Fig. 4g) appear as well. In the following cycles (Fig. 4h-j), the

signals from the α-Sn phase appear and vanish contemporaneously with the ß-Sn phase, indicating that the α-Sn phase gets lithiated and de-lithiated in a similar way as the ß-Sn phase. Figure 5 shows the XRD patterns and the result of the structural Rietveld refinement for the measurement, before and after the first charge/discharge cycle. Figure 5a shows the XRD pattern before the lithiation process starts. All detectable reflections can be assigned to the ß-Sn phase and the Be-window. After one complete cycle (see Figure 5b) three additional reflections appear. These reflections can be explained by the formation of the α-Sn phase. The results of the refinement are summarized in Table 1.

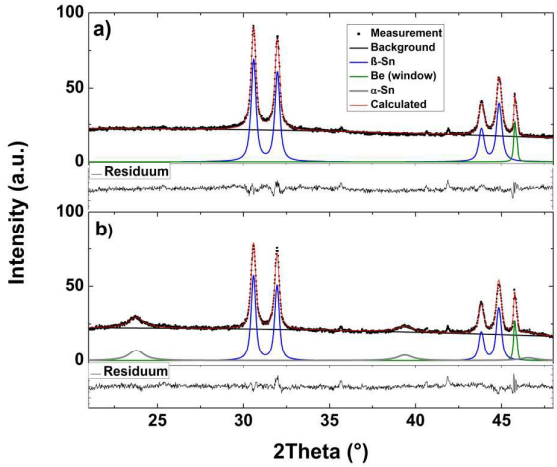

Figure 5: XRD measurement and refinement of the nano-Sn-based electrode before a) and after b) the first charge/discharge cycle.

The results of the refinement show that the crystallites of the α-Sn phase (L = 7.1(4) nm) are significantly smaller than the crystallites of the ß-Sn phase (L = 26(2) nm). The mean crystallite-size of the ß-Sn nanoparticles increases. Therefore we believe that the original size-distribution gets split into an α- and a ß-phase distribution. This observation is in conformity with earlier reports that the ß-/α-phase equilibrium depends on the size of the crystallites.[7] From the ratio of the peak intensities, we calculated the weight-ratio. Therefore, after one complete cycle, the crystalline part of the Sn nanoparticles consists of 19(1) wt.% α-Sn and 81(1) wt.% ß-Sn. Under the assumption that only the smallest particles in this distribution get transformed into the α-phase, one could calculate a critical size for the transformation of 11(3) nm. Our measurements show for the first time, that the α-Sn phase is formed already during the first charge/discharge cycle at 870 mV and simultaneously with the ß-phase.

Although the size-dependent phase transformation is very common for nanoparticle crystal structures, the phase transformation for Sn nanocrystals is poorly studied so far. Im *et al.*[5] used *ab initio* calculations to study the emergence of the α-phase. They concluded that once the α-phase is formed, it preserves its crystal structure, while the ß-phase is easily transformed into an amorphous phase during lithiation. Nevertheless, the formation of the α-phase is still supposed to be a size-related effect, which is not fully understood, so far. Beside the contribution of the surface energy, the formation and the stability of α-Sn depends on other factors as well. Gallerneault *et al.*[16] showed, that small amounts (0.6 wt.%) of Si can enhance the α-phase stability. Furthermore, a matrix is able to stabilize the α-Sn phase up to a melting point of 200°C.[17] However, there are no reports about the α-phase in Sn nanoparticles without the participation of lithium. Therefore, a lithium contribution to the α-phase formation should be considered as well. How the size of the crystallites, the incorporation of lithium and matrix-stabilization might affect the α-phase formation needs to be studied in future work.

Furthermore, the influence of the α-phase on the overall electrochemical performance of Sn-based anode materials needs to be examined more carefully. For example, Im *et al.*[5] reported that crystalline α-Sn can lead to an improved rate performance. However, α-Sn is a semiconductor and may lead to an increased internal resistance compared to metallic ß-Sn. Works by Kaghazchi[18–20] showed, that the insertion of Li in α-Sn is kinetically more favorable than in ß-Sn. Nevertheless, our measurement's show that the α-phase gets lithiated contemporaneous with the ß-Sn phase. Therefore the kinetically influence of Li insertion into the α-Sn phase seems to be negligible. Therefore, the insertion of lithium into the α-Sn phase as well as the effect of an increased electrical resistance need to be investigated more carefully and will be the topic auf our future work.

Conclusions

In conclusion, we could show for the first time by an *in situ* X-ray diffraction study that the α-Sn phase is formed already within the first cycle in a nano-particulate tin anode. The α-phase is formed simultaneously with the ß-Sn phase at a voltage of 870 mV. This α-phase gets lithiated in the next cycles similar to the ß-Sn phase. Furthermore, earlier observations about a critical-size of 17(4) nm could be confirmed within the experimental error. Although it is well known that unusual phase transformations in nanoparticles are size-related, one should consider that lithium insertion/extraction affects the formation and stability of the α-phase. The impact of the α-phase on the electrochemical performance of tin based anodes in a lithium-ion cell should be the topic of future research to gain a deeper insight into this, only little studied phase transformation.

Acknowledgements

The authors gratefully acknowledge funding of the EWE-Nachwuchsgruppe by EWE AG Oldenburg. Guido Schmuelling gratefully acknowledges funding of the project "Pouch-Zelle" (funding code: 64.65.69 – EM 1024 C) by the state NRW within the NRW Ziel 2-Programm (EFRE), Germany.

Notes and references

1 W.-R. Liu, Y.-C. Yen, H.-C. Wu, M. Winter and N.-L. Wu, *J. Appl. Electrochem.*, 2009, **39**, 1643–1649.
2 M. Winter, J. O. Besenhard, J. H. Albering, J. Yang and M. Wachtler, 1998, **17**.
3 C. Kim, M. Noh, M. Choi, J. Cho and B. Park, *Chem. Mater.*, 2005, **17**, 3297–3301.
4 L. Xu, C. Kim, A. K. Shukla, A. Dong, T. M. Mattox, D. J. Milliron and J. Cabana, *Nano Lett.*, 2013, **13**, 1800–1805.
5 H. S. Im, Y. J. Cho, Y. R. Lim, C. S. Jung, D. M. Jang, J. Park, F. Shojaei and H. S. Kang, *ACS Nano*, 2013, **7**, 11103–11111.
6 G. Schmuelling, N. Oehl, M. Knipper, J. Kolny-Olesiak, T. Plaggenborg, H.-W. Meyer, T. Placke, J. Parisi and M. Winter, *Nanotechnology*, 2014, **25**, 355401.
7 N. Oehl, L. Hardenberg, M. Knipper, J. Kolny-Olesiak, J. Parisi and T. Plaggenborg, *CrystEngComm*, 2015, **17**, 3695–3700.
8 J. M. McHale, A. Auroux, A. J. Perrotta and A. Navrotsky, *Science*, 1997, **277**, 788–791.
9 A. Navrotsky, *ChemPhysChem*, 2011, **12**, 2207–2215.
10 K. J. Rhodes, R. Meisner, M. Kirkham, N. Dudney and C. Daniel, *J. Electrochem. Soc.*, 2012, **159**, A294–A299.
11 N. Oehl, P. Michalowski, M. Knipper, J. Kolny-Olesiak, T. Plaggenborg and J. Parisi, *J. Phys. Chem. C*, 2014, **118**, 30238–30243.
12 H. Jia, C. Stock, R. Kloepsch, X. He, J. P. Badillo, O. Fromm, B. Vortmann, M. Winter and T. Placke, *ACS Appl. Mater. Interfaces*, 2015, **7**, 1508–1515.
13 J. R. Dahn, I. A. Courtney and O. Mao, *Solid State Ion.*, 1998, **111**, 289–294.
14 I. A. Courtney and J. R. Dahn, *J. Electrochem. Soc.*, 1997, **144**, 2045–2052.
15 C. Lupu, J.-G. Mao, J. W. Rabalais, A. M. Guloy and J. W. Richardson, *Inorg. Chem.*, 2003, **42**, 3765–3771.
16 W. M. T. Gallerneault, F. Vnuk and R. W. Smith, *J. Appl. Phys.*, 1983, **54**, 4200–4201.
17 M. F. Fyhn, J. Chevallier, A. N. Larsen, R. Feidenhans and M. Seibt, *Phys. Rev. B*, 1999, **60**, 5770.
18 P. Kaghazchi, *J. Phys. Condens. Matter*, 2013, **25**, 382204.
19 P. Kaghazchi, *J. Chem. Phys.*, 2013, **138**, 054706.
20 S. Sabet and P. Kaghazchi, *J. Chem. Phys.*, 2014, **140**, 191102.